CONF-861114--6

DE87 000882

Evidence for Correlated Double-Electron Capture in Slow Collisions of Multicharged Ions with He and H_2*

F. W. Meyer, C. C. Havener, R. A. Phaneuf, J.K. Swenson, S. M. Shafroth,[a] and N. Stolterfoht[b]

Oak Ridge National Laboratory, Oak Ridge, Tennessee 37831

Invited Paper to be presented at the
Ninth Conference on the Application of
Accelerators in Research and Industry
November 10-12, 1986
Denton, Texas

To be published in
Nuclear Instruments and Methods

---

*This work was sponsored by the Division of Chemical Sciences, U.S. Department of Energy, under Contract No. DE-AC05-840R21400 with Martin Marietta Energy Systems, Inc.

[a]Permanent address: University of North Carolina, Chapel Hill, N.C. 27514, and Triangle Universities Nuclear Physics Laboratory, Durham, N.C. 27706

[b]Permanent address: Hahn-Meitner-Institut für Kernforschung GmbH Berlin Glienickerstrasse 100, D-1000 Berlin 39, FRG.

DISCLAIMER

Evidence for Correlated Double-Electron Capture in Slow Collisions of Multicharged Ions with He and H_2

F. W. Meyer, C. C. Havener, R. A. Phaneuf, J.K. Swenson,[a] S. M. Shafroth,[a] and N. Stolterfoht[b]

Oak Ridge National Laboratory, Oak Ridge, Tennessee 37831

Abstract

High resolution measurements of the production of $L_1L_{23}M$ Coster-Kronig and LMM-Auger electrons in slow collisions of C^{4+}, N^{5+}, O^{6+}, and O^{7+} with He and H_2 have been performed, using the method of 0° Auger spectroscopy. For the latter three projectiles, strong Coster Kronig lines are observed, which are attributed to the configurations (core)2pnl, produced by double-electron capture. It is argued that production of these nonequivalent electron configurations must involve electron-electron correlation. From a comparison of the production cross sections for these Coster-Kronig electrons and the LMM-Auger electrons, it is further argued the correlation plays a significant role in two-electron transfer processes.

The study of two-electron capture by highly charged projectiles during slow collisions with few-electron targets such as He and H_2 is of considerable current interest. While the essential physics for single electron capture involving multicharged ions are now quite well understood, much remains to be learned about the role and importance of two-electron processes in low-energy, highly charged collision systems.

Crandall and coworkers[1] demonstrated about ten years ago the importance of double electron capture as a charge changing process in slow collisions of multicharged ions. Their experiment was based on detection of that fraction of product ions (i.e., projectile ions whose charge was reduced by 2) that survived the roughly microsecond flight time to the ion detector, and thus measured what has been referred to[2] as "true" double capture (TDC):

$$A^{q+} + He \rightarrow A^{(q-2)+*} + He^{2+} \qquad (1)$$

Measurements of TDC have been reported for a wide range of projectiles and targets.[3] TDC is the dominant channel for double capture from He in the case of incident projectiles having charge <4.

As the charge of the projectile ion increases, autoionizing double capture (ADC)

$$A^{q+} + He \rightarrow A^{(q-2)+**} + He^{2+} \qquad (2)$$
$$\hookrightarrow A^{(q-1)+} + He^{2+} + e$$

becomes significant, since the likelihood increases that both electrons are captured into excited states. This double capture channel has been observed, by Tsurubuchi et al.[4] for example, using the technique of translational spectroscopy. More recently Bordenave-Montesquieu et al.[5]

have energy analyzed the ejected electrons to obtain more detailed information on the doubly excited states formed in ADC. In addition, energy-gain spectra differential in scattering angle have been reported by Roncin et al.[2,6]

There is currently much discussion about the mechanisms involved in double electron capture. One focus of the discussion is the question of whether the two electrons are transferred independently (i.e., by two sequential one-electron transitions), or via a transition that involves electron-electron correlation and results in the simultaneous transfer of both electrons. The issue is illustrated schematically in Fig. 1, which shows potential curves for the A^{q+} + He collision system. Included in the figure are the dominant one electron transfer channel $A^{(q-1)+*}(n)$ + He^{+}, and two double capture exit channels leading to $A^{(q-2)+**}(n,n)$ + He^{2+} and $A^{(q-2)+**}(n',n'')$ + He^{2+}, respectively. As may be seen in the figure, there are two paths leading to the (n,n) double capture exit channel. The path shown as a dashed line illustrates the sequential one-electron capture route (crossings labelled 1 and 3) leading to the (n,n) final state, while the dotted line shows the route (crossing labelled 2) involving a single correlated two-electron transition. It should be noted that at energies in the vicinity of the cross section maximum for one-electron capture (into which range the energies of the present investigation fall), the probabilities for following either path at the one-electron transfer crossing (labelled 1) are comparable. Thus, both correlated double capture and sequential single capture are possible mechanisms for the creation of those states having at least one electron in the shell populated by single capture. It is therefore not straightforward to draw conclusions about the

role of correlation in the formation of these equivalent or near-equivalent electron configurations.

Consider now the second double capture exit channel in Fig. 1 leading to $A^{(q-2)+**}(n',n'')$. By analogy to the preceeding discussion relating to the (n,n) exit channel, it is evident that again there two possible paths leading to (n',n''), the first via crossings labelled 1 and 5, the second via crossing labelled 4. However, in this case, both paths now include transitions caused by electron correlation (i.e., include crossings of potential curves which differ by two spin orbitals). Observation of these so-called nonequivalent electron configurations populated in slow double capture collisions can therefore be interpreted as being direct evidence of electron correlation.

Such an observation was reported recently by Stolterfoht et al.,[7] who studied the production of LMM-Auger and $L_1L_{23}M$ Coster-Kronig electrons in slow O^{6+} + He collisions, using the method of 0° Auger spectroscopy. In the case of incident oxygen projectiles, strong Coster-Kronig lines were found, attributed to the configurations $1s^22pnl$ with $n>6$ which are produced by double capture. Since the dominant principal quantum number populated by single capture capture for this collision system is 3, these (nonequivalent) configurations correspond to the second case discussed above, and must thus involve a transition between potential curves that differ by 2 electron orbitals (i.e., caused by electron correlation). Also measured was production of LMM-Auger electrons resulting from the configurations $1s^23lnl'$ also produced by double capture. These equivalent or near-equivalent configurations correspond to the first case discussed in connection with Fig. 1, and can be formed either by two sequential single-electron

transitions or from correlated two-electron transfer. From a comparison of the cross sections for production of the Coster-Kronig and LMM-Auger electrons, respectively, the relative importance of the correlated double-capture process could be inferred.

In order to gain further insight into the dependence of $L_1L_{23}M$ Coster-Kronig and LMM-Auger electron production on projectile charge and target, electron spectra have also been measured for C^{4+} + He and H_2, N^{5+} + He and H_2, as well as for O^{7+} + He. Results of these measurement are presented below.

The measurements were carried out using the ORNL ECR ion source in conjunction with a 0° Auger spectroscopy apparatus temporarily transported from Hahn-Meitner Institut, Berlin. The ions of interest extracted from the multicharged ion source were magnetically anayzed and directed into a gas cell located in the scattering chamber. Electrons produced in the gas cell were measured at 0° observation angle by a tandem spectrometer consisting of two electrostatic parallel-plate analyzers, separated by an electron deceleration stage. The entrance analyzer was used to deflect the electrons out of the ion beam, and the exit analyzer determined the energy of the electrons with a resolution determined by the deceleration upstream of the final analyzer.

Care was taken to assure that the cross section measurements were obtained under single collision conditions. For selected cases measurements were made over a range of target-cell gas pressures. An example of such a pressure dependence measurement is shown in Fig. 2, where relative cross sections for the production of Coster-Kronig and LMM-Auger electrons,

respectively, for O^{6+} + He collisions are shown for a number of different target presssures.

Absolute cross sections were determined from the observed electron yields using methods previously described.[7] The Coster-Kronig electrons observed in the present investigation had laboratory energies as low as a few eV. Since such low energy electrons are easily disturbed by spurious instrumental effects, the gas cell was biased at -50 V to accelerate the electrons out of the target region. Possible focusing effects produced by the acceleration were investigated by varying the cell bias, and were found to be well within the 30% experimental uncertainty determined for the measured cross section.

Table I summarizes our cross section results for the production of $L_1L_{23}M$ Coster-Kronig electrons and LMM-Auger electrons. The cross sections refer to the projectile frame of reference, where the electron emission is assumed to be isotropic. A detailed discussion of these results will be presented elsewhere. The present discussion will be restricted to observations of some of the general features characterizing the measured electron energy spectra.

Figure 3 shows a comparison of the Coster-Kronig and LMM-Auger electron spectra for the O^{6+} + He collision system. The Coster-Kronig electron spectrum shows a well defined Rydberg series converging to a series limit at 12 eV. The lowest energy peak corresponds to n=6. The LMM Auger spectrum, on the other hand, is comprised of many lines, whose precise identification will require detailed atomic structure calculations. The LMM Auger spectrum is characterized by two broad groupings of lines. The first group falls in the electron energy range 20 - 40 eV, and originates

from $1s^2 3131'$ configurations, while the second falls in the range 40 - 65 eV, and originiates from $1s^2 3141'$ configurations. Reference to Table I shows the Coster-Kronig and LMM-Auger production cross sections for this collision system to be of the same order of magnitude.

Figure 4 shows the Coster-Kronig electron spectra for C^{4+} incident on He and H_2, respectively. In the He target case, production of the Coster-Kronig electrons is found to be suppressed. This observation is explained by the fact that in the C^{4+} + He collision system, the $1s^2 2pnl$ channels are endothermic, and thus do not have favorable crossings with the entrance channel (see Fig. 3 in Ref. 9). In the case of the C^{4+} + H_2 system, on the other hand, such crossings exist due to the reduced ionization potential of the target, and, as is evident in Fig. 4, result in strong Coster-Kronig lines. The production of $1s^2 2pnl$ nonequivalent electron configurations thus is seen to depend strongly on the collision partners, and can be understood on the basis of the potential curve crossing model implied in Fig. 1.

To illustrate the effect of projectile charge, Fig. 5 shows Coster-Kronig spectra for N^{5+} and O^{7+} incident on He. The difference in electron energies at which the (core)2pnl series limit occurs, reflects the difference in 2s-2p splittings for the two ions, ΔE_{2s2p}. The line energies are well described by the relation $\epsilon = \Delta E_{2s2p} - B_n$, where B_n is the binding energy of the Rydberg electron given by RQ^2/n^{*2}. The quantity Q is the effective nuclear charge, n* involves the quantum defect, and R is the Rydberg constant. Table I summarizes the threshold principal quantum numbers above which the Coster-Kronig electrons are energetically allowed for the collision systems studied.

In summary, we have shown that the study of Coster-Kronig electrons originating from the nonequivalent electron configurations (core)2pnl that are populated by double capture collisions provide a direct method for observing correlation effects in two-electron-transfer processes. From a comparison of the production cross sections for these Coster-Kronig electrons with those for the LMM-Auger electrons, it is seen that electron-electron correlation plays a significant role in two-electron transfer processes involving highly charged ions.

This work was sponsored by the Division of Chemical Sciences, U.S. Department of Energy, under Contract No. DE-AC05-84OR21400 with Martin Marietta Energy Systems, Inc.

References

[a]Permanent address: University of North Carolina, Chapel Hill, N.C. 27514, and Triangle Universities Nuclear Physics Laboratory, Durham, N.C. 27706

[b]Permanent address: Hahn-Meitner-Institut für Kernforschung GmbH Berlin Glienickerstrasse 100, D-1000 Berlin 39, FRG.

1. D. H. Crandall, R. E. Olson, E. J. Shipsey, and J. C. Browne, Phys. Rev. Lett. 36, 858(1976).

2. P. Roncin, M. Barat, H. Laurent, J. Pommier, S. Dousson, and D. Hitz, J. Phys B 17, L521 (1984).

3. E.g., S. Bliman, J. Aubert, R. Geller, B. Jacquot, and D. Van Houtte, Phys. Rev. A 23, 1703 (1981); Cuneyt Can, Tom J. Gray, S. L. Varghese, J. M. Hall, and L. N. Tunnell, Phys. Rev. A 31, 72 (1985).

4. S. Tsurubuchi, T. Iwai, Y. Kaneko, M. Kimura, N. Kobayashi, A. Matsumoto, S. Ohtani, K. Okuno, S. Takagi, and H. Tawara, J. Phys. B 15, L733 (1982).

5. A. Bordenave-Montesquieu, P. Benoit-Cattin, A. Gleizes, A. I. Marrachi, S. Dousson, and D. Hitz, J. Phys. B 17, L127 (1984), J. Phys. B 18, L195 (1985), J. Phys. B 17, L223 (1984).

6. P. Roncin, H. Laurent, and M. Barat, J. Phys. E 19, 37 (1986).

7. N. Stolterfoht, C. C. Havener, R. A. Phaneuf, J. K. Swenson, and S. M. Shafroth, Phys. Rev. Lett. 57, 74 (1986).

Table I. Auger electron production cross section results; 10 × q keV projectile energies

Projection	Target	Production Cross Section (10^{-17} cm^2)		
		(core)2pnℓ	n	(core)3ℓn'ℓ'
C^{4+}	He	<0.5	4	—
C^{4+}	H_2	3.8	4	3.7
N^{5+}	He	2.2	5	2.2
N^{5+}	H_2	8.0	5	25
O^{6+}	He	3.3	6	5.4
O^{7+}	He	3.3	9	17

Figure Captions

Fig. 1. Schematic potential curves for the A^{q+} + He collision system.

Fig. 2. Pressure dependences of the Coster-Kronig (top) and LMM-Auger (bottom) electron production cross sections for O^{6+} + He.

Fig. 3. Comparison of the Coster-Kronig (top) and LMM-Auger (bottom) electron spectra for O^{6+} + He.

Fig. 4. Comparison of the Coster-Kronig electron spectra for C^{4+} incident on He and H_2. For both targets raw spectra as well as background stripped spectra are shown. The latter are used to determine absolute cross sections.

Fig. 5. Coster-Kronig electron spectra for N^{5+} and O^{7+} incident on He.

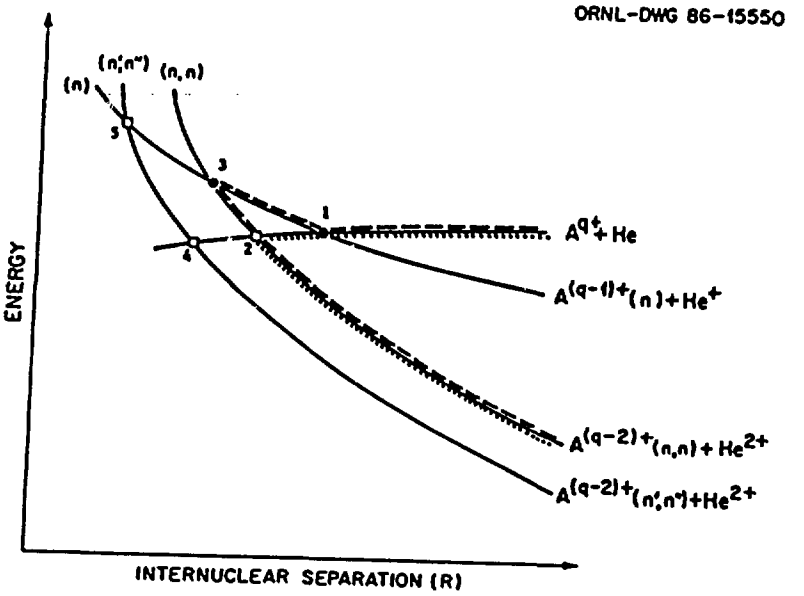
ORNL-DWG 86-15550
(n;n")
(n,n)
(n)
5
3
1
2
4
ENERGY
$A^{q+}+He$
$A^{(q-1)+}(n)+He^{+}$
$A^{(q-2)+}(n,n)+He^{2+}$
$A^{(q-2)+}(n';n")+He^{2+}$
INTERNUCLEAR SEPARATION (R)

Fig. 1

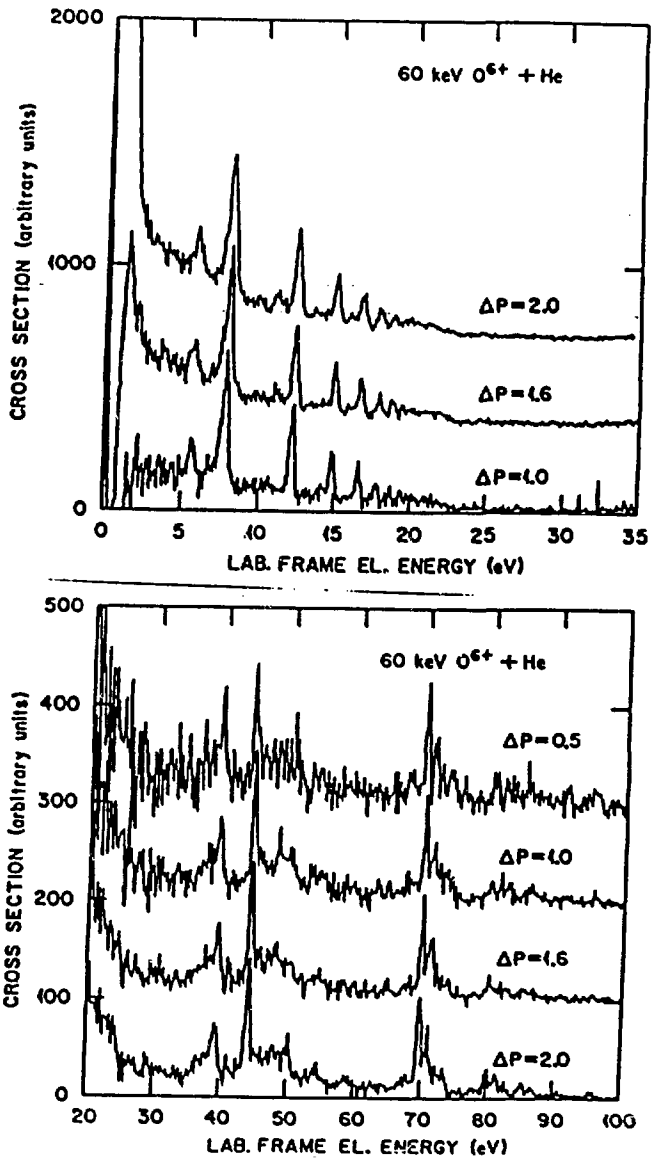
60 keV O^{6+} + He
ΔP=2.0
ΔP=1.6
ΔP=1.0
CROSS SECTION (arbitrary units)
LAB. FRAME EL. ENERGY (eV)
60 keV O^{6+} + He
ΔP=0.5
ΔP=1.0
ΔP=1.6
ΔP=2.0
CROSS SECTION (arbitrary units)
LAB. FRAME EL. ENERGY (eV)

Fig. 2

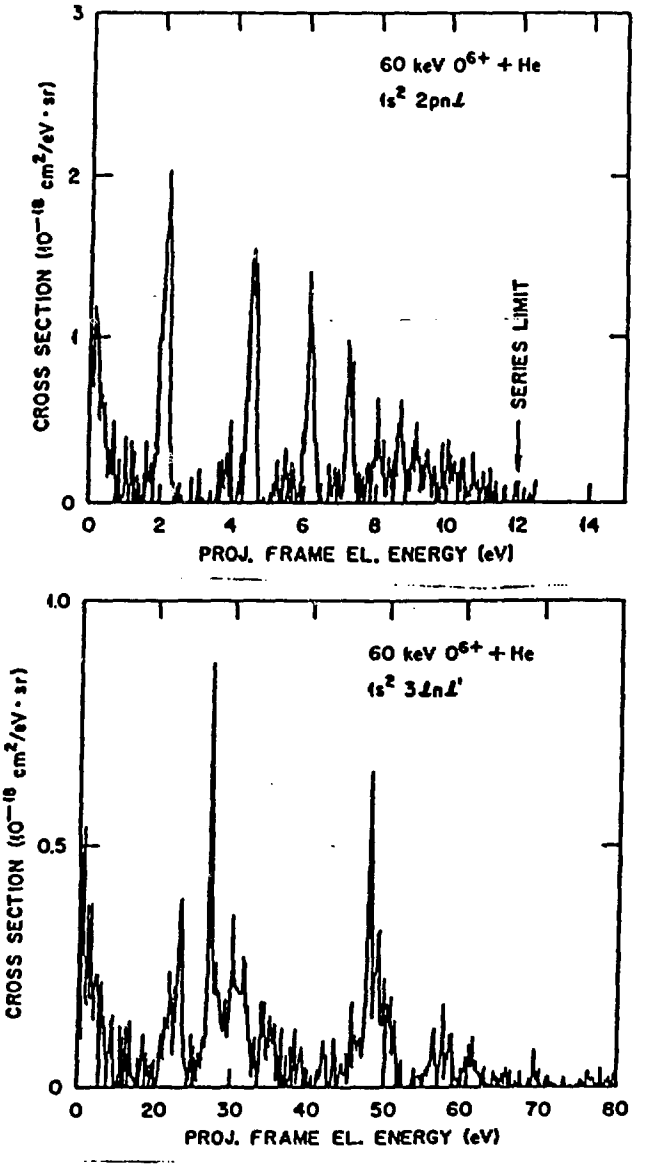
60 keV O^{6+} + He
$1s^2$ 2pnℓ
SERIES LIMIT
CROSS SECTION (10^{-18} cm²/eV · sr)
PROJ. FRAME EL. ENERGY (eV)
60 keV O^{6+} + He
$1s^2$ 3ℓnℓ'
CROSS SECTION (10^{-18} cm²/eV · sr)
PROJ. FRAME EL. ENERGY (eV)

Fig. 3

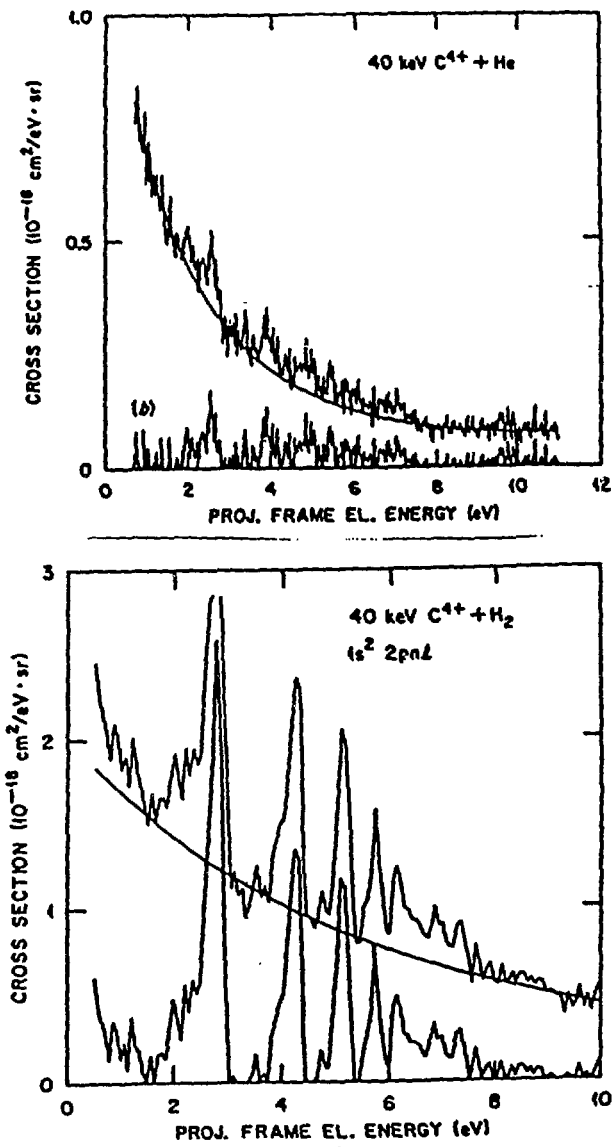
40 keV C4+ + He
(b)
CROSS SECTION (10⁻¹⁸ cm²/eV·sr)
PROJ. FRAME EL. ENERGY (eV)
40 keV C4+ + H2
1s² 2pnℓ
CROSS SECTION (10⁻¹⁸ cm²/eV·sr)
PROJ. FRAME EL. ENERGY (eV)

Fig. 4

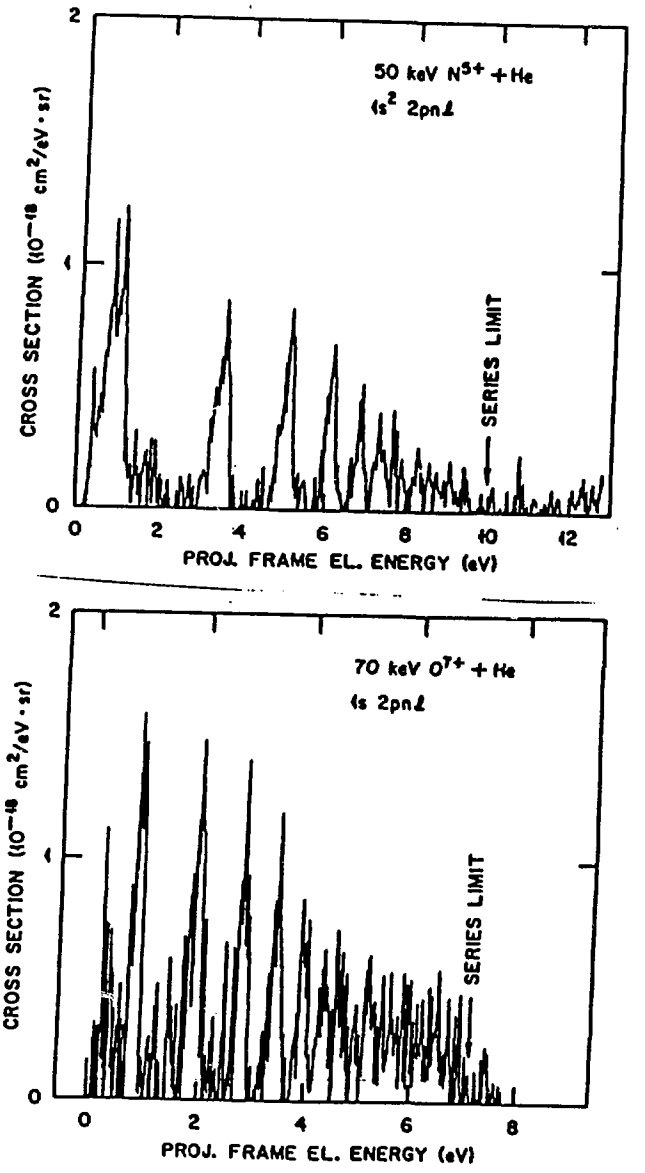
50 keV N^{5+} + He
$1s^2$ 2pnℓ
SERIES LIMIT
CROSS SECTION (10^{-18} cm²/eV · sr)
PROJ. FRAME EL. ENERGY (eV)
70 keV O^{7+} + He
1s 2pnℓ
SERIES LIMIT
CROSS SECTION (10^{-18} cm²/eV · sr)
PROJ. FRAME EL. ENERGY (eV)

Fig. 5